



Galvanic Cr-Zn and spent foundry sand waste application as valuable components of sustainable ceramics to prevent environment pollution

Vsevolod Mymrin¹ · Simone C. Borgo² · Kirill Alekseev¹ · Monica A. Avanci¹ · Paulo H. B. Rolim¹ · Marco A. Argenda² · Walderson Klitzke² · Alexandre J. Gonçalves¹ · Rodrigo E. Catai¹

Received: 8 October 2019 / Accepted: 31 January 2020 / Published online: 24 February 2020
© Springer-Verlag London Ltd., part of Springer Nature 2020

Abstract

The purpose of this study was to develop new composites of glass-ceramics from hazardous Cr-Zn galvanic sludge (up to 30%), spent foundry sand (25%), glass rejects from metal surface cleaning (20%), and natural red clay (25%) to produce environmentally clean ceramics. All the raw materials and the developed ceramics were analyzed by XRF, XRD, DTA and TGA, SEM, AAS, and LAMMA. The ceramics showed very high flexural resistance (up to 22.84 MPa) and low values of linear shrinkage (5.02%), water absorption (3.20%), and bulk density (2.00 g/cm³) after sintering at temperatures of 950–1200 °C for 1 h. The solubility and leaching of heavy metals from the developed composites with 75% of industrial wastes were far below Brazilian standards, which makes them eco-friendly materials. Such properties allow the use of the ceramics for the production of facing tiles, roof tiles, blocks, and bricks with high economic efficiency.

Keywords Hazardous galvanic sludge · Spent foundry sand · Surface cleaning glass rejects · Heavy metal leaching/solubility · Environment-friendly ceramics

1 Introduction

Galvanic process plants are one of the most widely distributed industries all over the world. Residues from these industries usually contain high levels of heavy metals, such as Ni, Zn, Cr, Sn, Cu, Pb, and Sb. About 4000 industries in EU countries produced 150,000 tons/year of galvanic sludge [14]. Economic valuation studies of the sludge from the galvanization process were carried out due to its great polluting potential and had concluded that the cost of the sludge disposal is near US\$ 250.00 per ton [1]. Industrial waste dumps pollute the environment, including groundwater [7]. Novak et al. [24] studied a number of shallow aquifers in industrial regions polluted by toxic Cr(VI) and spontaneous reduction of

dissolved Cr(VI) to insoluble Cr(III). The studies of Warchulski et al. [31] were the first attempt to apply a combination of electromagnetic measurements and mineralogical investigations to pyrometallurgical heavy metal slags of the Upper Silesia region of Poland, and to precisely describe links between the obtained conductivity and in-phase results and phase building soils and sediments of the studied area. A significant number of international publications demonstrate the possibility of employing heavy metals from galvanic waste inertization to interrupt environmental pollution. One of the most popular methods of galvanic sludge processing is the heavy metal recovery: up to 95% Cu recovery using acid solutions with heating at 110 °C [28]; Vilarinho and Ribeiro [30] increased the recovery and purity rate of Cu and Ni up to 99%. Sodium sulfite and ferrous sulfate can be used [8] as a reducing agent with 100% efficiency. Bratskaya et al. [3] reduced the heavy metal contents by the Zn²⁺, Cu²⁺, and Ni²⁺ removal from a solution by a flocculation/precipitation process using a chitosan derivative. New biotechnology researches (bioleaching and biosorption) for heavy metal recovery were discussed by Cui and Zhang [5]. Levitskii and Poznyak [12] realized that the inclusion of 9% of galvanic

✉ Vsevolod Mymrin
seva6219@gmail.com

¹ Federal University of Technology, Deputado Heitor Alencar Furtado str, 4900, Ecoville, Curitiba, PR, Brazil

² Federal University of Paraná, Curitiba, PR, Brazil

sludge affects the thermophysical characteristics, reducing the thermal conductivity and mechanical resistance. It was studied by Mymrin et al. [19] applicability and viability of galvanic sludge in composites with oil-contaminated diatomite waste and glass waste in red ceramic fabrication.

Brazil generates more than 3 million tons of waste foundry sand annually, making it one of the largest industrial wastes produced in the country. The main part of foundry sand (FS) is thrown into the factory industrial dumps [16]. Spent FS is a waste of liquid metal casting from the machine construction industry, where sand is used in molding operations, becoming polluted by the chemical elements of these metals. Annual estimates indicate that the quantity of FS is approximately 100 million tons; the main part of FS is thrown into the factory industrial dumps [2].

A total analysis for Ag, Al, Ba, Be, Cd, Co, Cr, Cu, Fe, Mg, Mn, Mo, Ni, Pb, Sb, Te, Tl, V, and Zn was conducted by Miguel et al. [17] on 96 foundry sands and 14 native soils collected from 17 small- and medium-sized foundries in Argentina. Ceramic production is a highly promising method of using hazardous foundry sand. Mymrin [18] employed FS in composites with different types of hazardous industrial wastes to produce environmentally clean ceramics, particularly, hazardous laundry sewage sludge in composites with kaolin clay. Pytel [26] pulled metals apart from FS and applied for ceramic production. Furlani et al. [9] added FS to red or yellow clay for ceramic fabrication. It was developed by Raupp-Pereira et al. [27] ceramics from foundry sand in blends with sewage sludge, aluminum anodizing sludge, and marble sawing sludge. Matos et al. [16] proposed the use of FS in two ways: in conventional concrete by WFS calcination and in dry mix concrete for the production of concrete blocks.

According to Nishida et al. [23], glass wastes (GW) are an advantageous medium for stable solidification of heavy metal ions (Cr, Fe, Cu, Zn, and Pb). It was studied [20] new ceramic composites from sewage sludge, foundry sand, glass waste, and acid neutralization salts. The results showed that the ceramic sintered at 1050 °C achieved flexural strength of up to 18.4 MPa, low values of water absorption and linear shrinkage, thus demonstrating the efficiency of this composite.

There are many processes for abovementioned industrial waste utilization, but virtually most part of them are economically unprofitable, and they remain environmentally hazardous. Therefore, the current study aimed to (1) develop new composites from two types of galvanic wastes (galvanic sludge and surface metal cleaning glass waste), foundry sand with the insertion of a single natural material—local red clay—to produce environmentally clean ceramics; (2) investigate the processes of the new ceramic structural formation, responsible for obtaining the mechanical properties; and (3) develop an ecologically safe method of ceramic production in laboratory scale with the potential of converting it into a pilot scale.

2 Raw materials and methods

2.1 Raw materials

In this research, industrial wastes such as galvanic sludge (GS), metal cleaning GW, and FS were used. The only natural component, local red clay, was used as a plasticizer for these wastes' mixtures and as a binder at low temperatures. All components of this study were collected nearby the city of Curitiba, Brazil; the clay was taken from a career near the city of Curitiba; the GS and GW were obtained in the galvanic plant "Tecnoplating"; a machine construction enterprise provided the FS sample.

2.2 Methods

All raw materials and developed ceramics were characterized by the following methods: the particle size distribution was evaluated by the sieve method; chemical composition by XRF with a Philips/PANalytical, model PW 2400; mineralogical composition by XRD with a Philips, model PW 1830 with the radiation $\lambda_{\text{Cu-K}\alpha}$ and diffractogram patterns analyzed with the High Score software, using the PDF-2 databank. Thermal analyses, using the DTA and TGA methods, were performed at a heating rate of 10 °C/min until 1226 °C in an air atmosphere and natural cooling with the automatically turned off furnace. The morphological structures were studied by SEM, applying a JEOL JSM-6360 LV, and micro-chemical composition by EDS with a JEOL JSM-5410 LV. The LAMMA method was used to investigate the isotopic composition of the developed ceramics (with a LAMMA-1000, model X-ACT). The solubility and lixiviation of heavy metals were determined by AAS method, using a Perkin Elmer 4100 device. The values of the ceramic flexural resistance strength were obtained in equipment for destructive mechanical tests model EMIC, DL-10. The basic physical properties of the ceramics, such as water absorption, linear shrinkage, and bulk density of the ceramics in the heating temperatures, were also determined.

2.3 Preparation of the ceramic test samples

The preparation of the test samples (TSs) of the ceramics followed the subsequent steps: (1) homogenization of all dry components in different percentages, previously predetermined; (2) dry mixture's hydration with water content between 12 and 14%; (3) compaction of the hydrated mixture at a 5-MPa pressure using traditional rectangular molds of 60 × 20 mm sizes; (4) drying to a constant TS weight at 100 °C; (5) firing with a heating rate of 10 °C/min until 950°, 1000°, 1050°, 1100°, 1150°, and 1200 °C with exposure for 1 h at maximum temperature and self-cooling in the automatically switched off oven. All physical properties were

calculated with average and standard deviations of 10 replications; therefore, the total quantity of the test specimens was approximately 400 pieces.

2.4 Calculations

Flexural resistance of the ceramics was calculated using the formula:

$$R_f = [(3 \cdot c \cdot d) / (l \cdot h^2)] \tag{1}$$

where R_f = flexural resistance (MPa); c = maximum load reached at the moment of rupture (kgf) adjusted with a speed of 0.5 mm/min; d = distance between the supports of the test piece (mm); l = width of the test piece (mm); and h = height of the test piece (mm).

Water absorption (W_a) of TSs was determined at room temperature, comparing the sample weight before and after submersion in potable water for 24 h:

$$W_a(\%) = [(M_h - M_d) / M_d] \cdot 100 \tag{2}$$

where W_a (%) = water absorption (%), M_h = mass after submersion body (g); and M_d = mass before submersion specimen (g).

3 Research results

3.1 Raw material characterization

The characterization of all the raw materials under study consisted of their granulometric, chemical and mineralogical compositions, and morphological microstructure with the aims of to select (1) the combinations of components and their ratios with maximum values of mechanical properties and (2) to study the influence of all component on the structure formation processes of the materials.

3.1.1 Particle size distribution of the raw materials

Analysis of the raw materials’ particle size distribution by the sieve method (Table 1) showed that the foundry sand was the coarsest component, with 66.39% of particles between 0.29

and 0.15 mm, followed by glass waste and galvanic sludge that presented respectively 30.28% and 11.15% of particles in the same size range.

3.1.2 The chemical composition of the raw materials (by XRF method)

There was a considerable disparity in the chemical (Table 2) and mineralogical compositions of the industrial wastes under scrutiny.

The dominant components of the GS (Table 2) were heavy metals (Cr 28.53 and Zn 20.28 wt%) with a total amount of 48.78%. The comparative GS, used by Magalhaes et al. [13], held 11.71% of heavy metals. Heavy metals were also present in GW and FS, but in a lesser quantity (1.21%). The total sum of heavy metals of all wastes under study in the galvanic process was 51.99%. GW consisted mainly of SiO₂ (75.50%) and alkaline components, Na₂O (10.13%), K₂O (8.50%), CaO (8.46%), and MgO (3.04%). Foundry sand had almost pure SiO₂ (98.75%). The chemical composition of natural clay contained 54.50% CaO, 21.42% Al₂O₃, 8.33% Fe₂O₃, 4.98% K₂O, and 2.34% SO₃. High-iron chromium-based slag was used by Zhang et al. [32] to prepare an iron-rich CaO-MgO-Al₂O₃-SiO₂ glass-ceramics.

3.1.3 Mineral composition of the raw materials (by XRD method)

The XRD diffractogram pattern of galvanic sludge (Fig. 1a) comprised X-ray background with two halos of amorphous materials and their extremums at approximately 35° and 61° of 2θ of λCu-Kα. Only a very weak crystal peak of the SiO₂ quartz crystalline structure was found at the top of the second amorphous halo at 2θ = 61°. The XRD diffractogram pattern of glass waste (Fig. 1b) also consisted of amorphous material with one robust and vast amorphous halo from 12° to 38° of 2θ of λCu-Kα, typical of vitreous structures. In contrast, the XRD pattern of foundry sand (Fig. 1c) had a sizeable SiO₂ quartz crystal structure advantage over amorphous. The total intensity of the entire FS diffraction pattern (3600 counts per second) was about 36 times higher than the intensity of the diffraction patterns of GS and GW (100 counts per second). Only quartz has been detected; the high content of amorphous material was masked by the high intensity of the crystal peaks.

Table 1 Particle size distribution (%) of the raw materials

mm/%	1.19–0.6	0.59–0.3	0.29–0.15	0.14–0.075	0.074–0
Galvanic sludge	0	2.31	11.15	30.08	56.46
Foundry sand	0	14.63	66.39	17.63	1.35
Glass waste	0	6.32	30.28	49.21	14.19
Natural clay	0	1.39	3.17	5.68	89.76

Natural clay was the finest material due to the number of primary particles (89.76%) smaller than 0.074 mm

Table 2 Principal elements of the chemical composition of the raw materials (by XRF and AAS methods)

No.	Components, wt%				No.	Components, wt%			
	Wastes under study			Clay		Wastes under study			Clay
	GS	GW	FS			GS	GW	FS	
SiO ₂	12.53	75.50	98.75	54.50	Cu	0.53	0	0	0
CaO	6.03	8.46	0	4.05	Se	0.31	0	0	0
MgO	2.80	3.04	0	1.53	Co	0.26	0	0	0
Al ₂ O ₃	2.25		0.31	21.42	Ni	0.24	0	0	0
Fe ₂ O ₃	4.31	0.69	0.41	8.33	W	0.21	0	0	0
P ₂ O ₅	8.22	0.97	0	0.17	Sn	0.21	0	0	0
Na ₂ O	2.70	10.13	0	1.45	Pb	0.21	0.02	0	0
K ₂ O	1.44	8.50	0	4.98	Sr	0	0.02	0	0
SO ₃	8.94	0.26	0	2.34	I ₂ O ₃	0	0.92	0	0
Cr	28.53	0.02	0	0					
Zn	20.28	0.07	0	0	I.L.	41.82	0.45	0.53	7.91

I.L. ignition loss

An intermediate position in the ratio of crystalline and amorphous structures was occupied by the natural clay sample (Fig. 1d). NC was represented by an approximately equal number of crystalline structures of quartz and the clay-crystalline illite

mineral; the X-ray background intensity of NC practically coincided with the background intensity of GS and GW.

3.1.4 Morphological structure of the raw materials

Galvanic sludge is a product of the electrochemical destruction of metal surfaces. Therefore, after drying and grinding, GS (Fig. 2a) was represented by particle aggregates of very complex chemical compositions (Table 2). These aggregates and the pores between them had different sizes and shapes. The spent glass waste consisted predominantly of glass microspheres (Fig. 2b), either whole or fractured during the metal surface cleaning. The particle diameter of the spheres varied between 60 and 250 μm , and the broken particles between 1 and 50 μm . The foundry sand sample (Fig. 2c) enclosed rounded particles of irregular shape, varying in size mainly from 150 to 400 μm . As a rule, they were covered with a mechanically disturbed scaly layer both during geological epochs and during temperature shocks of the casting processes. The natural clay (Fig. 2d) exhibited shapeless particles with a large number of scaly particles with jagged, broken edges. The largest particle sizes did not exceed 20 μm .

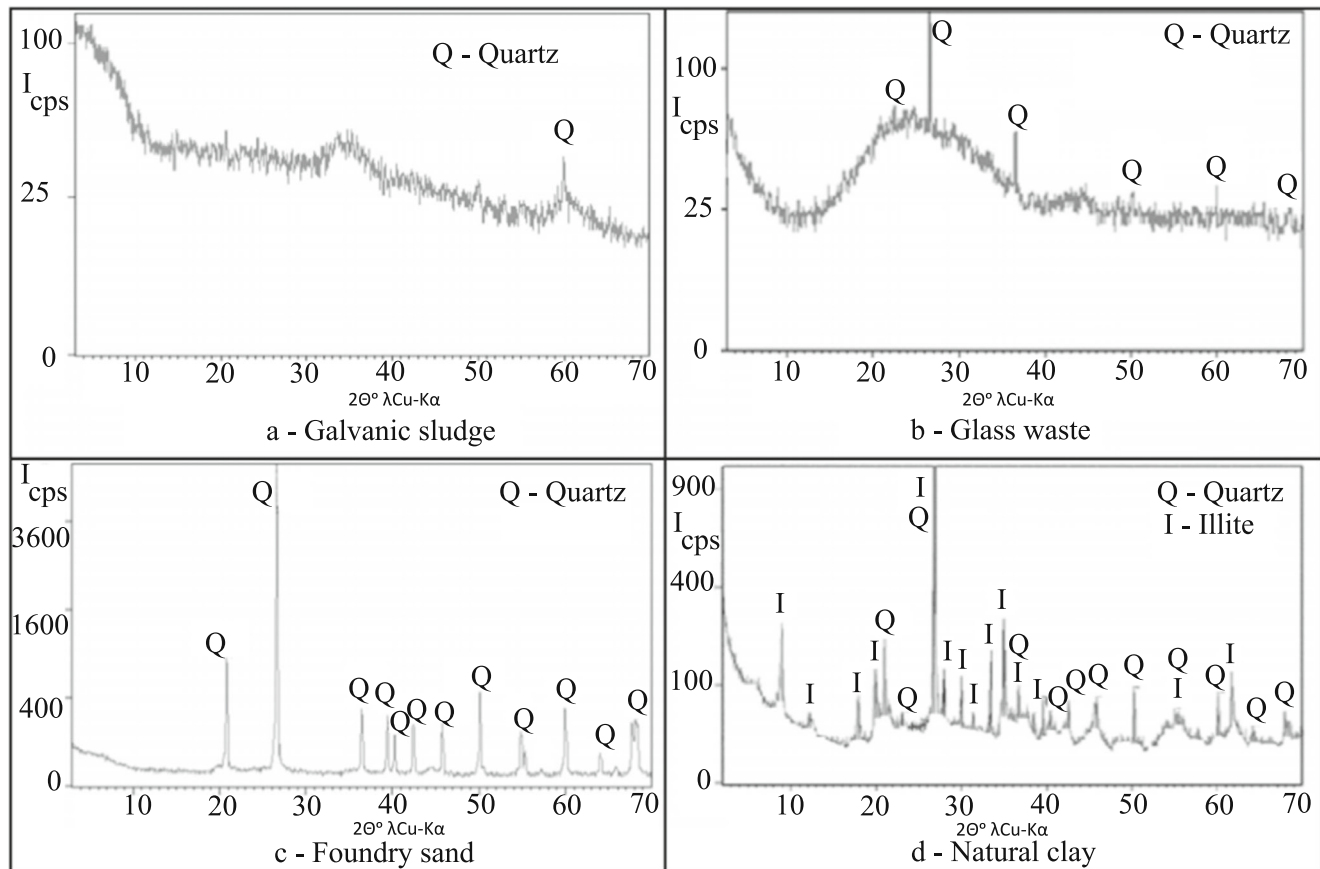
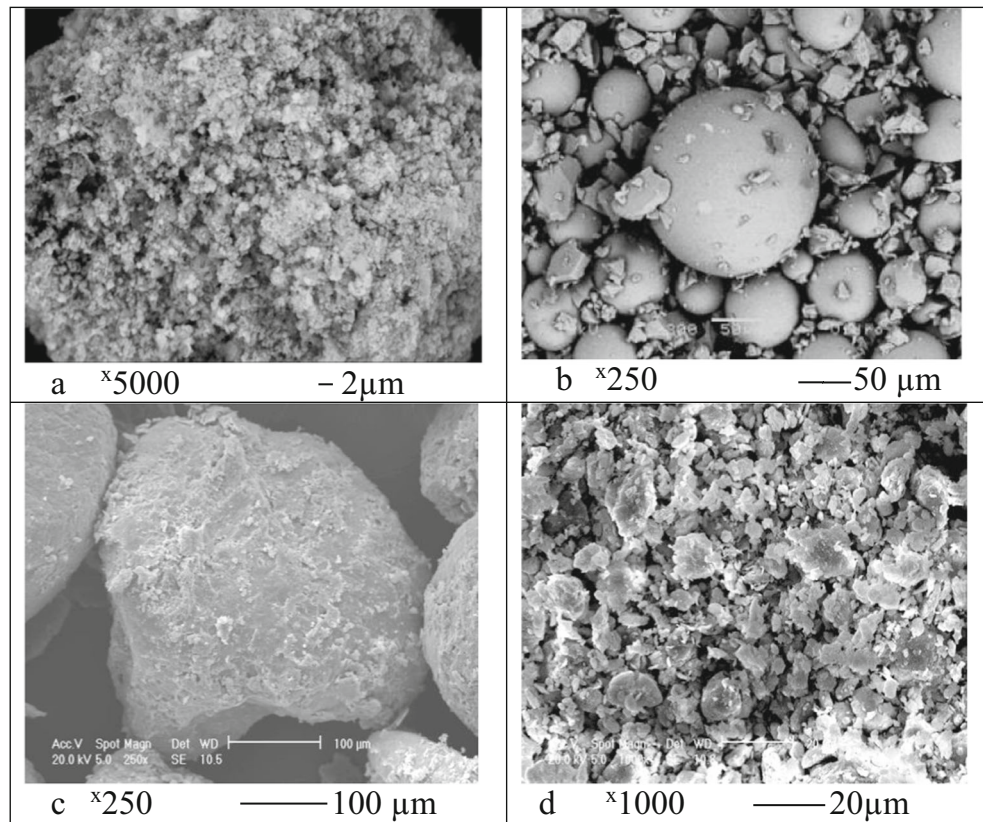


Fig. 1 XRD patterns of the raw materials. **a** Galvanic sludge. **b** Glass waste. **c** Foundry sand. **d** Natural clay

Fig. 2 SEM micro-images of the raw materials. **a** Galvanic sludge. **b** Glass waste. **c** Foundry sand. **d** Clay



3.2 Physical properties of the clay-waste ceramics

The mechanical and physical properties of all developed ceramics were studied after firing between 950 and 1200 °C; the physicochemical processes of structure formation were investigated only after firing of ceramic 6.

The studied waste-clay ceramics’ structure formation physical properties were flexural resistance, shrinkage, water absorption, and bulk density of ceramics during firing at 950°–1200 °C.

3.2.1 Changes in flexural resistance of clay-waste ceramics sintered at different temperatures

Table 3 data showed the direct relationship between the flexural resistance of the ceramics and the galvanic sludge content

and the sintering temperature until 1150° (compositions 1–3) or 1100 °C (compositions 4–6). Such difference might be explained by the increase of the galvanic sludge content from 5 to 15% in ceramics 1–3 and up to 20–30% in ceramics 4–6 due to the expansion in the number of heavy metals with lower melting points: Zn (419.4 °C), Mg (650 °C), Al (658 °C), Ca (838 °C), Cu (1083 °C), serving as fluxes. Ceramic 6 with maximum residue content (75%), particularly with maximum galvanic sludge content (30%) and minimum values of clay (25%), presented the highest resistance value (22.84 MPa). The melting point of composite 6 was between 1100 and 1150 °C with a corresponding decrease in resistance from 22.84 to 14.48 MPa, ensued by the complete sample’s melting at 1200 °C. The ceramics 4–6 formed rounded edges in the specimens at 1100 °C and began to glow. The ceramics’ color

Table 3 Flexural resistance of ceramics sintered at different temperatures

No.	Compositions (wt%)				Flexural resistance (MPa) of ceramics sintered at <i>T</i> (°C)					
	GS	FS	GW	NC	950	1000	1050	1100	1150	1200
1	5	25	20	50	4.62	6.20	11.28	14.81	16.64	15.45
2	10	25	20	45	4.27	5.83	12.42	15.63	17.20	16.38
3	15	25	20	40	3.95	5.40	13.80	17.44	18.62	16.21
4	20	25	20	35	3.52	5.54	15.37	19.87	18.49	13.20
5	25	25	20	30	2.79	5.32	16.40	20.92	17.20	12.13
6	30	25	20	25	2.57	4.84	17.63	22.84	14.48	0

changed from a light brown at 950 °C to a dark brown at 1100 °C.

Ceramic 1 with a maximum content of natural clay (50%) had the best flexural resistance values at low temperatures, 4.62 and 6.20 MPa at 950 and 1000 °C correspondingly; resistance values of 6.20 MPa signify a 55% surplus of the maximum demand (4 MPa) of Brazilian standards [22] for building ceramics, such as bricks and blocks.

The decrescent clay content in composites 2–6 raised the resistance values, although with a significant increase in heating temperature. The resistance of ceramic 1 composition began to yield to the resistance of ceramic 2, with a 5% higher waste content, only after an increase in the firing temperature of 50 and 100 °C. Therefore, for industrial use, the maximum amount of clay is desired. The 50% content of hazardous industrial wastes in composite 1 was also an excellent result regarding the environment.

3.2.2 Changes in linear shrinkage of clay-waste ceramics sintered at different temperatures

The changes in the shrinkage of the clay-waste ceramics (Table 4) widely agreed with the changes in their strength (Table 3). Undeniable direct relation of the linear shrinkage of ceramics 1–3 to the sintering temperature up to 1150 °C and up to 1100 °C for ceramics 4–6.

Ceramics of all composites began to expand after these temperatures due to excessive melting. An increase in the industrial waste fraction with a decrease in clay contents led to excessive melting at lower temperatures. Ceramic 1, with the highest clay and lowest waste contents, showed the highest shrinkage values at each firing temperature due to the lower heavy metal's contents.

3.2.3 Changes in the water absorption of clay-waste ceramics sintered at different temperatures

The water absorption values (WA) of the ceramics (Table 5) illustrated their continuous reduction along with the growth of the sintering temperatures and the decrease in the natural clay contents.

The total WA decrease was from 23.17% (composite 1 after sintering at 950 °C) to 2.11% (composite 5 at 1200 °C), which far exceeds the requirements (8%) of the Brazilian norms NBR 15270-3/050 [22]. The WA coefficient is an indirect indicator of the open porosity of the material. Consequently, from the results listed in Table 5, it became evident how the open porosity decreases with the firing temperature [25]. This was derived from both the softening of the initial mixture's particles and their adhesion and due to the accelerated chemical interaction between them with increasing temperature.

3.2.4 Changes in the bulk density of clay-waste ceramics sintered at different temperatures

The bulk density values of ceramic 1 increased steadily (Table 6) until firing at 1200 °C. The density of ceramics 2 and 3 grew only up to the temperature of 1150 °C and strikingly decreased at 1200 °C. The same event occurred with the samples of compositions 4, 5, and 6, however after heating at a temperature of 1100 °C. This change sequence in density values imparted the change in linear shrinkage values of the same samples (Table 4). This fact might explain the lowering of the clay-waste shrinkage with the reduction in clay content from composition 1 to composition 6. The slowing down of the samples' shrinkage indicated the beginning of the reverse process—their expansion due to excessive melting.

This also manifested itself at the beginning of the process of rounding the corners and edges of ceramics; roundness increased with temperature. The samples' resistance dropped sharply (Table 3), especially at a temperature of 1200 °C, and the samples of ceramic 6 melted entirely. GSW-clay composites also showed lower open porosity.

3.3 Physicochemical processes of the clay-waste ceramic structure formation

The samples of the developed ceramic materials were studied by XRD, DTA and TGA, SEM, EDS, and LAMMA methods after their firing at 950 and 1100 °C in order to understand the reasons for achieving such values of the physical properties. Composition 6 was chosen to investigate the physicochemical

Table 4 Linear shrinkage (%) of ceramics after sintering at different temperatures

No.	Compositions (wt%)				Linear shrinkage (%) of ceramics after sintering at T (°C)					
	GS	FS	GW	NC	950	1000	1050	1100	1150	1200
1	5	25	20	50	2.42	3.37	5.29	7.12	11.67	10.32
2	10	25	20	45	2.24	3.14	5.15	6.95	7.45	6.30
3	15	25	20	40	2.12	3.03	5.02	6.43	6.27	5.14
4	20	25	20	35	2.03	2.84	4.91	6.37	5.16	4.05
5	25	25	20	30	1.86	2.63	4.80	5.16	4.72	3.02
6	30	25	20	25	1.74	2.35	4.72	5.02	4.14	0

Table 5 Water absorption of ceramics after sintering at different temperatures (°C)

No.	Compositions (wt%)				Water absorption (%) of ceramics sintered at T (°C)					
	GS	AF	GW	NC	950	1000	1050	1100	1150	1200
1	5	25	20	50	23.17	22.65	21.54	18.83	12.69	8.24
2	10	25	20	45	21.15	19.15	17.35	13.48	9.14	6.24
3	15	25	20	40	19.45	18.09	12.15	10.76	8.65	5.83
4	20	25	20	35	17.34	15.26	11.20	7.88	6.25	4.17
5	25	25	20	30	14.62	10.71	7.53	5.16	4.03	2.11
6	30	25	20	25	11.78	8.86	5.14	3.20	2.15	Melted

processes of the clay-waste ceramics' structure formation, since it presented the lowest natural material content—clay (25%), the highest strength values (Table 3), and the highest industrial waste content (75%), especially the most dangerous among them—galvanic sludge (30%, Table 2).

3.3.1 Mineralogical composition of composite 6 fired at 900 and 1100 °C

Comparison of XRD patterns of the starting raw materials (Fig. 1) with those of ceramic 6 (Fig. 3a) after firing at 950 °C showed a complete change in the mineral composition of the initial mixture due to the chemical interaction of the components in an alkaline environment with high heavy metal contents at high temperatures. The complete disappearance of the crystalline peaks of illite $KAl_2(Si,Al)_4O_{10}(OH)_2nH_2O$ was observed. The only resemblance to the original components' diffraction patterns was a very high content of the amorphous phase and mineral quartz SiO_2 , which was present in all components.

The SiO_2 peak intensity strongly increased due to the high content (25%) of the remarkably crystalline foundry sand (Fig. 1c) and possibly to the partial crystallization of a highly concentrated amorphous silicon component. The only new crystal structures synthesized after firing the initial mix at 900 °C were a small amount of nepheline $(Na,K)AlSiO_4$.

The increase of the firing temperature to 1100 °C (Fig. 3b) conducted to significant growth of both crystalline and amorphous phases. An increase in the quartz and nepheline peak

intensity caused a doubling of the intensity scale from 1000 to 2000 counts per second; the peaks of the cristobalite SiO_2 (high-temperature modification of quartz) and the new mineral albite $NaAlSi_3O_8$ became visible. The X-ray background also doubled, reflecting the quantity of amorphous mass. The study of such materials allowed Deubener et al. [6] to offer a revised, updated definition of glass-ceramics, which reads “Glass-ceramics are inorganic, non-metallic materials prepared by controlled crystallization of glasses via different processing methods. They contain at least one type of functional crystalline phase and a residual glass. The volume fraction crystallized may vary from ppm to almost 100%.”

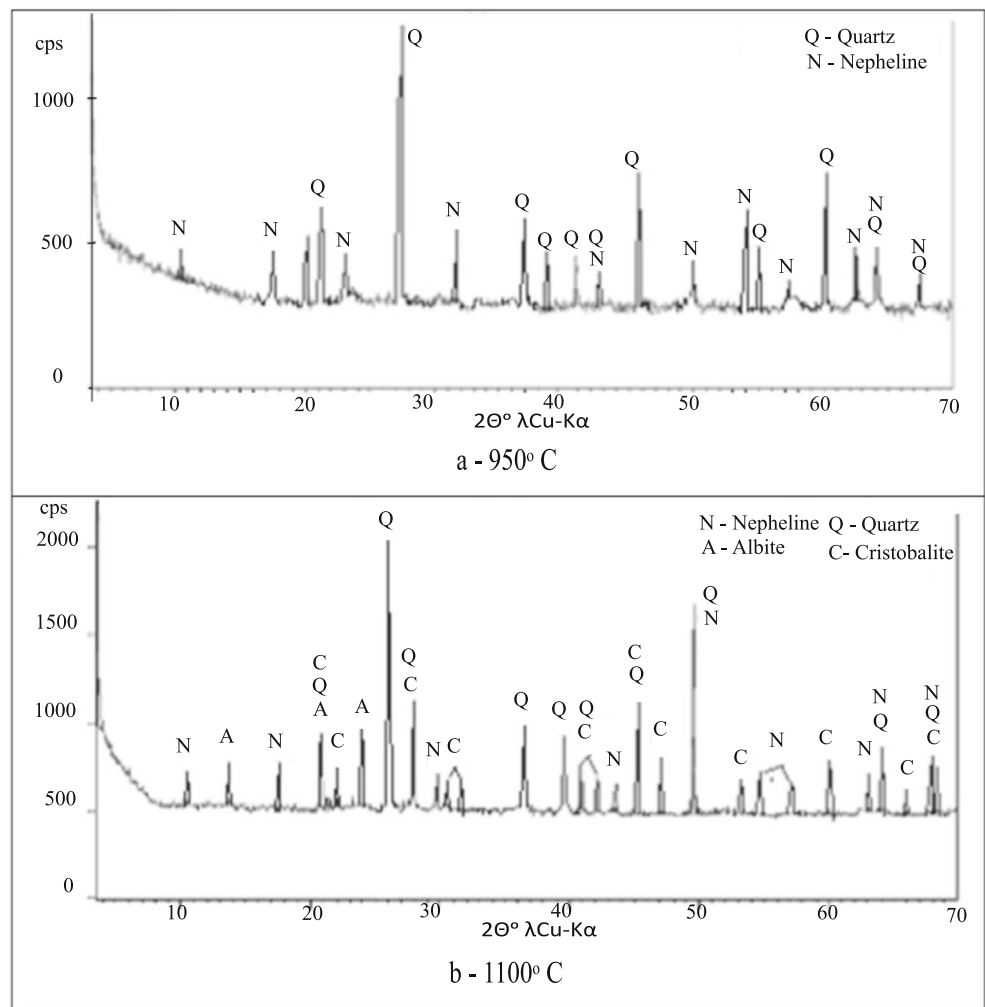
3.3.2 Thermochemical reactions during composite 6's firing at 900 and 1100 °C

The composition 6 consisted of 30% galvanic sludge, 25% foundry sand, 20% waste glass, and 25% natural clay. The chemical interactions of these components, during heating until 1226 °C, presented on the DTA and TGA curves (Fig. 4) were introduced in the form of two small endothermic effects and a large exothermic one. The first endothermic effect, located at 22–201 °C, represented the evaporation of the pores and weakly bonded waters as 6.84% weight loss. The second endothermic effect, between 201 and 285 °C, indicated the transition of $Al(OH)_3$ to $\gamma-AlO(OH)_4$ [4] with 4.28% weight loss. The remainder of the thermal curve, at 285–1226 °C, showed the exothermic effect with 5.18% weight loss,

Table 6 The bulk density of ceramic compositions at different firing temperatures

No.	Compositions (wt%)				Density (g/cm^3) of ceramics sintered at T (°C)					
	GS	FS	GW	NC	950	1000	1050	1100	1150	1200
1	5	25	20	50	1.19	1.27	1.48	1.51	1.74	1.85
2	10	25	20	45	1.33	1.42	1.57	1.69	1.81	1.78
3	15	25	20	40	1.45	1.58	1.69	1.75	1.85	1.70
4	20	25	20	35	1.58	1.61	1.78	1.90	1.83	1.64
5	25	25	20	30	1.65	1.70	1.84	1.99	1.87	1.53
6	30	25	20	25	1.78	1.83	1.94	2.00	1.92	Melted

Fig. 3 XRD patterns of the ceramic 6 after firing at **a** 950 °C and **b** 1100 °C



paradigmatic for the transition of anhydrous $\gamma\text{-Al}_2\text{O}_3$ to $\alpha\text{-Al}_2\text{O}_3$ [10, 11]. The process of organic residues burning in foundry sand took place with the formation of different types of gases [15]. Waste glass underwent the amorphous

phase crystallization process [29]; the result of these processes in composition 6 was that it began to melt, after firing at 1100 °C, and its flexural strength fell from 22.84 to 14.48 MPa, at 1150 °C. Similar effects

Fig. 4 DTA and TGA curves of composite 6

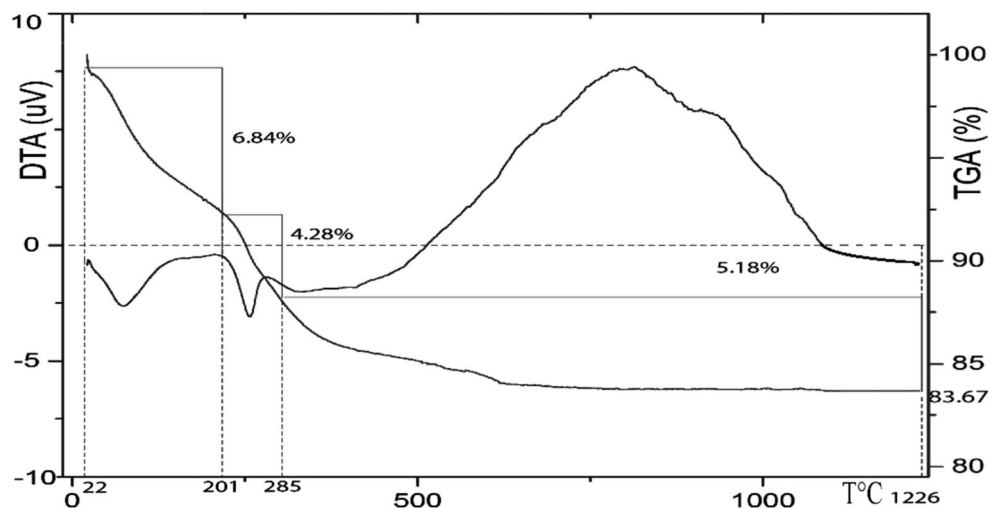
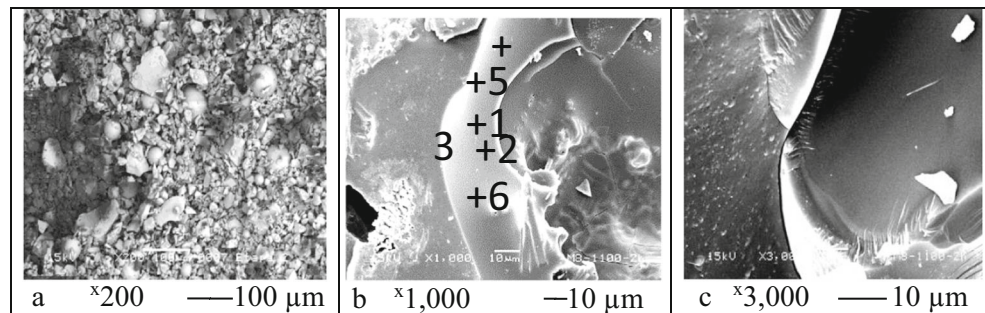


Fig. 5 SEM micrographs. **a** Initial mixture of components before the firing. **b, c** Glass-like new formations after the firing



of sintering temperature on crystallization and phase change, micromorphology, and physical-chemical properties of glass-ceramics were investigated also by Zhenget et al. [33].

3.3.3 Morphological structure of ceramic 6 fired at 1100 °C

SEM micrographs of the initial mixture of components prior to firing (Fig. 5a) showed the presence of segregated particles of different sizes and forms.

Glass waste particles might be recognized among those as microspheres or fragments thereof. The initial mixture of the composition 6 was represented by particles of different sizes and shapes; only particles of spent glass waste have predominantly micro-sphere form of different diameters, varying in size mainly from 20 to 50 μm. All particle had no some bonding between them with a large number of pores also of various sizes and configurations. The micro-level of the ceramic's surfaces (Fig. 5b, c) after firing at 1100 °C was presented by new molten glass-like formations, very different from the initial ones (Fig. 5a). There were no longer visible particles from the original components in the SEM micrographs. All of them were partially melted and amalgamated (physical interaction) or simultaneously involved in a much faster and more complex chemical interaction at high temperatures. Illite initial crystal structures were utterly melted and transferred to amorphous conditions. It was still possible to find some micropores in SEM micrographs; however, they were scarce and, mainly, closed pores. Such changes from tangled original mix to glass-like structure granted a sharp drop in water adsorption

values (Table 5) from 11.78 to 3.20% and an increase in resistance from 2.57 to 22.84 MPa (Table 3) during firing from 950 to 1100 °C.

3.3.4 The micro-chemical composition of ceramic 6

The micro-chemical composition of the total area (Table 7) of ceramic 6 shown in Fig. 5c revealed robust consistency with the average chemical composition of all raw materials (Table 2). Nevertheless, all six separate points did not have the faintest similarity in the percentages of each chemical element, including the first three points that were as close as possible to each other (approximately 10 μm). This fact indicated a very high level of heterogeneity in the chemical composition of ceramics, characteristic of amorphous materials. The very high complexity of the chemical composition of the initial mixtures of all compositions (Table 2) following the Groth crystal-chemical law (the more complex the chemical composition, the lower the symmetry, and vice versa) also prevented the synthesis of crystalline structures. A paltry number of synthesized crystals of nepheline and albite, seen at different points of the samples (Fig. 3), failed to affect the structure and properties of the ceramics meaningfully.

Similar results were obtained using laser micro-mass analyses (LAMMA) (Fig. 6), which showed the isotope composition of individual points of ceramic 6 after firing at 1100 °C. Both the mass number of the isotopes and their content (relative intensity) at three points closer to each other had a massive difference. This difference, as well as the EDS results (Fig. 5c, Table 7), indicated a high heterogeneity of the

Table 7 EDS spectra of the total area and 6 points (Fig. 6c) of composition 6 after firing at 1100 °C

Area, points	Na	Mg	Al	Si	P	K	Ca	Cr	Fe	Zn	Total
Area	3.37	2.15	6.26	60.36	2.22	3.53	5.42	7.21	4.35	5.13	100.0
1	2.53	–	19.65	3.56	2.23	19.33	1.52	12.77	2.23	36.18	100.0
2	3.54	2.39	3.37	9.62	16.74	18.85	4.38	36.43	2.52	2.14	100.0
3	–	2.03	2.43	1.00	45.03	0.48	5.46	9.15	6.67	27.75	100.0
4	8.16	0.17	–	20.17	0.16	5.02	3.99	24.76	2.39	35.18	100.0
5	2.01	0.25	2.56	7.00	6.21	10.37	1.19	3.43	20.44	46.54	100.0
6	5.00	2.01	4.59	0.53	0.47	1.14	6.20	68.14	1.17	10.75	100.0

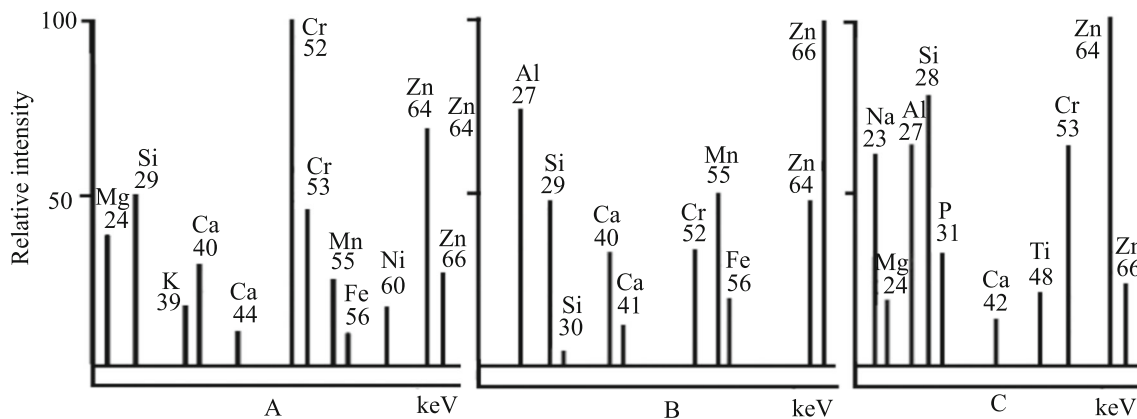


Fig. 6 a–c Isotopic composition of the nearest points of the ceramic 6 fired at 1100 °C

chemical composition of the sample points, which is characteristic of glass-like amorphous materials.

3.4 Environmental characteristic of ceramic 6

Leaching tests of the fired products evaluated the environmental risks of the incorporation of GSW, rich in heavy metals (Cr, Zn, Ni, and others), to a clay matrix (Table 8).

The results indicated a successful inertization of the pollutants [21]. In order to control the environmental impact of the developed composites, ceramic 6 was chosen on account of the highest industrial waste content (75%), holding predominantly the most hazardous waste used in the study (30% of galvanic sludge) and the lowest natural clay content (25%). The determination of the values of lixiviation and solubility of heavy metals from the

ceramic 6 after firing at 1100 °C (Table 5) was carried out in acid solutions in accordance with NBR 10.004 [21].

The comparison of the values of heavy metal lixiviation and solubility from ceramic 6 with the requirements of NBR 10.004 [21] showed a robust advantage of the obtained results. These values were much lower than the sensitivity of the atomic absorption analyses (AAS). It has been assumed that the demand for other heavy metals' lixiviation and solubility would have a similar reserve of advantage.

4 Conclusions

1. The study results showed the empirical odds of employing a rather small (25%) amount of natural red clay to resolve a significant environmental problem caused by hazardous industrial wastes, using them as valuable raw materials to produce environmentally clean ceramics. The industrial wastes under study were galvanic sludge (up to 30%) carrying Cr and Zn, spent foundry sand (25%), and metal surface cleaning glass reject (20%) with extremely high (50.78 wt%) total heavy metal content.
2. The developed composites, fired at 950–1150 °C, presented high values of physical properties: flexion resistance up to 22.84 MPa, linear shrinkage up to 5%, water absorption up to 3.20%, and bulk density up to 2.00 g/cm³. Therefore, they might be used for the manufacture of environmentally clean construction materials such as facing tiles, roof tiles, blocks, bricks, and others.
3. Such characteristics were obtained due to the sintering of mainly glassy structures of the ceramics with small inclusions of nepheline (Na,K)AlSiO₄, albite NaAlSi₃O₈, quartz SiO₂, and cristobalite SiO₂. On account of the glassy structure, the ceramics presented very reduced values of lixiviation and solubility of heavy metals in acidic solutions, much smaller than the standard requirements.
4. The developed materials should be highly economically attractive because of the content of up to 75% of industrial

Table 8 Lixiviation and solubility of heavy metals from the developed ceramics

Elements	Leaching (mg/L)		Solubility (mg/L)	
	Comp. 6	NBR*	Comp. 6	NBR*
As	0.21	1.0	<0.001	0.01
Ba	2.04	70.0	0.018	0.7
Cd	0.03	0.5	0	0.005
Pb	0.15	1.0	<0.01	0.01
Cr total	0.78	5.0	0.01	0.05
Hg	0.02	0.1	<0.001	0.001
Se	0.12	1.0	<0.001	0.01
Al	0.17	**	0.03	0.2
Cu	0.05	**	0.24	2.0
Fe	0.86	**	0.04	0.3
Mn	0.18	**	0.03	0.1
Zn	0.02	**	0.27	5.0

*NBR 10.004 [21]

**Demands have not been established yet by Brazilian standard

wastes for producing construction materials. A considerable decrease in the costs is further enhanced by the following: (a) fourfold reduction in the use of relatively expensive and in some places inaccessible natural clay; (b) low prices of the raw materials—industrial wastes (or with surcharge from manufacturers of hazardous industrial wastes and with free shipping for their transportation).

5. The wide-scale use of the method is environmentally effective as its most important advantage is the use of industrial wastes that contaminate the environment, reducing the open-quarry extraction of natural components of construction materials—clay and sand.

Acknowledgments The authors are grateful to the staff from the Laboratory of Analyses of Minerals and Rocks (LAMIR) of Federal University of Paraná, Curitiba, Brazil, for technical support in providing chemical and mineralogical analyses.

References

- Alves LC, Seo ESM (2014) Characterization of the solid residue from the process for environmental economic valuation. *J Environ San Eng* 19:423–434. <https://doi.org/10.1590/S1413-41522014019000000637> (in Portuguese)
- Bhimani DR et al (2013) A study on foundry sand: opportunities for sustainable and economical concrete. *J Int Glob Res Anal* 2:1 https://www.worldwidejournals.com/global-journal-for-research-analysis-GJRA/file.php?val=January_2013_1358501392_37069_25.pdf
- Bratskaya SY et al (2009) Heavy metals removal by flocculation/precipitation using N-(2-carboxyethyl) chitosans. *J Colloids Surf A* 339:140–144. <https://doi.org/10.1016/j.colsurfa.2009.02.013>
- Brown ME, Gallagher PK (2011) Handbook of thermal analysis and calorimetry: recent advances, techniques and applications. Elsevier. <https://books.google.com.br/books?hl=pt-BR&lr=&id=0TjcPYVDNSEC&oi=fnd&pg=PP1&dq=Brown,+M.E.,+Gallagher,+P.K.,+2011,+Handbook+of+thermal+analysis+and+calorimetry:+recent+advances,+techniques+and+applications.+Elsevier.&ots=yCvG1P6pul&sig=HsrSS4CrQOPWCSv-WXMNzVoYUUG#v=onepage&q=Brown%2C%20M.E.%2C%20Gallagher%2C%20P.K.%2C%202011.%20Handbook%20of%20thermal%20analysis%20and%20calorimetry%3A%20recent%20advances%2C%20techniques%20and%20applications.%20Elsevier.&f=false>
- Cui J, Zhang L (2008) Metallurgical recovery of metals from electronic waste: review. *J Hazard Mater* 158:228–256 <https://www.sciencedirect.com/science/article/pii/S0304389408002161?via%3Dihub>
- Deubener, J., et al, 2018. Updated definition of glass-ceramics J. *Non-Crystalline Solids* 501, 3–10. <https://doi.org/10.1016/j.jnoncrysol.2018.01.033>
- Economou-Eliopoulos M (2017) Geochemical constraints on the sources of Cr (VI) contamination in waters of Messapia (Central Evia) Basin. *J Appl Geochem* 84:13–25. <https://doi.org/10.1016/j.apgeochem.2017.05.015>
- Erdem M, Tumen F (2004) Chromium removal from aqueous solution by the ferrite process. *J Hazard Mater* 109:71–77. <https://doi.org/10.1016/j.jhazmat.2004.02.031>
- Furlani E et al (2014) Preparation and characterization of sintered ceramics made with spent foundry olivine sand and clay. *J Ceram Int* 38:2619–2625. <https://doi.org/10.1016/j.ceramint.2011.11.065>
- Johnson DW, Gallagher PK (1971) Kinetics of the decomposition of freeze-dried aluminum sulfate and ammonium aluminum sulfate. *J Am Ceram Soc* 54:461–465
- Kato E et al (1981) Decomposition of two aluminum sulfates and characterization of the resultant aluminas. *J Am Ceram Soc* 64(8): 436–443
- Levitskii IA, Poznyak AI (2015) Thermophysical characteristics of furnace tiles obtained using galvanic production wastes. *J Glass Ceram* 72:130–134
- Magalhaes JM et al (2004) Physical and chemical characterization of metal finishing industrial wastes. *J Environ Manag* 75:157–166. <https://doi.org/10.1016/j.jenvman.2004.09.011>
- Magalhães JM et al (2005) Role of the mixing conditions and composition of galvanic sludges on the inertization process in clay-based ceramics. *J Hazard Mater* 106:169–176
- Maryandyshev PA et al (2016) Thermal decomposition and combustion of coals, fuel wood, and hydrolytic lignin, as studied by thermal analysis. *J Solid Fuel Chem* 50:167–176. <https://doi.org/10.3103/S0361>
- Matos PR et al (2019) Novel applications of waste foundry sand in conventional and dry-mix concretes. *J Environ Manag* 244:294–303. <https://doi.org/10.1016/j.jenvman.2019.04.048>
- Miguel RE et al (2012) Analysis of total metals in waste molding and core sands from ferrous and non-ferrous foundries. *J Environ Manag* 110:77–81. <https://doi.org/10.1016/j.jenvman.2012.05.025>
- Mymrin V. Industrial and municipal wastes utilization as economical and environment efficient raw materials. <http://paginapessoal.utfpr.edu.br/mymrinev>. Accessed 18 March 2012. (in Portuguese)
- Mymrin V et al (2013) Oily diatomite and galvanic wastes as raw materials for red ceramics fabrication. *Constr Build Mater* 41:360–364. <https://doi.org/10.1016/j.conbuildmat.2012.11.041>
- Mymrin V et al (2016) Influence of kaolin clay on mechanical properties and on the structure formation processes of white ceramics with inclusion of hazardous sewage sludge. *J Appl Clay Sci* 155:95–102. <https://doi.org/10.1016/j.clay.2018.01.006>
- NBR 10.004 (2004) Solid wastes - classification. Rio de Janeiro, 2004 (in Portuguese)
- NBR 15270-3/05 (2005) Flexural rupture strength and water adsorption measurement of ceramic bricks, Rio de Janeiro (in Portuguese)
- Nishida T et al (2000) Solidification of hazardous heavy metal ions with soda-lime glass—characterization of iron and zinc in the waste glass. *J Ceram Soc Jpn* 108:245–248
- Novak M et al (2017) Chromium isotope fractionations resulting from electroplating, chromating and anodizing: implications for groundwater pollution studies. *J Appl Geochem* 80:134–142. <https://doi.org/10.1016/j.apgeochem.2017.03.009>
- Pérez-Villarejo L et al (2012) Manufacturing new ceramic materials from clay and red mud derived from the aluminum industry. *Constr Build Mater* 35:656–665. <https://doi.org/10.1016/j.conbuildmat.2012.04.133>
- Pytel Z (2014) Evaluation of potential applications of recycled moulding and core sands to production of ceramic building materials. *J Ceram Int* 40:4351–4358
- Raupp-Pereira F et al (2007) Extrusion and property characterisation of waste-based ceramic formulations. *J Eur Ceram Soc* 275: 2333–2340. <https://doi.org/10.1016/j.jeurceramsoc.2006.07.015>
- Sethu VS, Aziz AR, Aroua MK (2008) Recovery and reutilization of copper from metal hydroxide sludge. *J Clean Technol Environ Policy* 10:131–136. <https://doi.org/10.1007/s10098-007-0133-4>
- Verheijen OS (2003) Thermal and chemical behavior of glass forming batches. Technische Universiteit Eindhoven. <https://doi.org/10.6100/IR565202>
- Vilarinho C, Ribeiro FA (2011) Small sized pilot scale experiments on the recovery copper and nickel hydroxide from galvanic sludge. <http://hdl.handle.net/1822/14997>

31. Warchulski R et al (2019) Rainwater-induced migration of potentially toxic elements from a Zn–Pb slag dump in Ruda Śląska in light of mineralogical, geochemical and geophysical investigations. *J Appl Geochem* 109:104396. <https://doi.org/10.1016/j.apgeochem.2019.104396>
32. Zhang W et al (2018) Crystallization mechanism and properties of glass ceramics from modified molten blast furnace slag. *J Non-Cryst Solids* 502:164–171. <https://doi.org/10.1016/j.jnoncrysol.2018.08.024>
33. Zhenget WM et al (2019) Thermal process and mechanism of phase transition and detoxification of glass-ceramics from asbestos tailings. *J Non-Cryst Solids* 517:26–31. <https://doi.org/10.1016/j.jnoncrysol.2018.10.029>

Publisher's note Springer Nature remains neutral with regard to jurisdictional claims in published maps and institutional affiliations.